Electrochemically Assisted Deposition of Calcite for Application in Surfactant Adsorption Studies

Haaring, Robert; Kumar, Naveen; Bosma, Duco; Poltorak, Lukasz; Sudhölter, Ernst J.R.

DOI
10.1021/acs.energyfuels.8b03572

Publication date
2019

Document Version
Final published version

Published in
Energy and Fuels

energy&fuels

Article

Cite This: Energy Fuels 2019, 33, 805−813

pubs.acs.org/EF

Electrochemically Assisted Deposition of Calcite for Application in Surfactant Adsorption Studies

Robert Haaring, Naveen Kumar,* Duco Bosma, Lukasz Poltorak,* and Ernst J. R. Sudhölter

Section Organic Materials & Interfaces, Department of Chemical Engineering, Delft University of Technology, Van der Maasweg 9, 2629 HZ Delft, The Netherlands

Supporting Information

ABSTRACT: The ability to study the adsorption behavior of surfactant species is of interest in the field of enhanced oil recovery (EOR), especially pertaining to alkaline surfactant flooding. In this work, a calcite model mineral surface was obtained by electrochemically assisted deposition. This was achieved via the nitrate and/or oxygen electroreduction reactions in the presence of bicarbonate and calcium ions, by which controlled deposition of calcium carbonate was effected on a quartz crystal microbalance sensor covered with an electroactive gold layer. In addition, the effect of pH and Ca^{2+} concentration on the effective surface charge of the deposited calcite particles was mapped. Calcite-modified sensors were used in conjunction with a quartz crystal microbalance with dissipation monitoring to study the effect of Na^{+} and Ca^{2+} concentration on the adsorption behavior of an anionic alcohol alkoxy sulfate (AAS) surfactant. Adsorption of the surfactant remained indifferent to ionic concentrations around the isoelectric point of calcite. Still, electrostatics play an important role in this regard, and it is essential to decrease the Ca^{2+} concentration sufficiently to minimize AAS adsorption. The results from this study show that a relatively simple method allows for the controlled deposition of a model rock surface, and there is ample opportunity to extend the work to other metal oxide surface types, including complex mixtures as can be obtained by co-deposition. Furthermore, the findings from these adsorption studies aid in the determination of optimal flooding parameters, with the aim to increase the efficiency and efficacy of EOR.

1. INTRODUCTION

Surfactant flooding is an enhanced oil recovery (EOR) technique, which employs surfactants to lower the interfacial tension between crude oil and water[1] and/or alter the wettability of the mineral surface to a more water-wet state.[2] One of the leading issues of surfactant flooding is the loss of surfactant through adsorption to porous rock surfaces in the petroleum reservoir.[3,4] As a result, the effectiveness of surfactant flooding on recovery suffers, and the process becomes economically unattractive. It is therefore important to investigate the governing factors regarding surfactant adsorption to mineral surfaces, in order to design the most optimal flooding parameters.

The major surface types in oil reservoirs are sandstones and carbonates. It is estimated that over half of the Earth's oil reservoirs are of a carbonate type,[5] and these usually have poorer recovery than sandstone reservoirs.[6] Thence, numerous studies on oil recovery and surfactant adsorption to silicates and carbonates have been carried out in the past.[7−14] Points of focus in these studies are, for example, the study of the effect of the brine/electrolyte in surfactant flooding on surfactant adsorption,[7,9,13] the employment of polyelectrolytes as sacrificial agents,[10,14] and the comparison of synthetic to natural rock surfaces and its effect on adsorption.[11] Adsorption studies on carbonates can be particularly challenging because of the chemical reactivity of this mineral compared to silica.

Within the framework of this study, surfactant adsorption to the rock surface is affected, among others, by three prominent factors: (1) surface composition and its pH-dependent surface charge, (2) composition of the flooding solution, and (3) surface heterogeneity. This motivates to map the mineralogy of an oil reservoir before choosing (the parameters for) a flooding technique. Aside from the inherent (electro)chemical properties of the surface, the environmental conditions are also a contributing factor to the effectiveness of surfactant flooding.

It has been shown before that the properties of mineral oxides depend strongly on pH,[10,15] and as such the ζ-potential may vary drastically among different reservoir conditions. For example, depending on the pH, the ζ-potential of calcite and metal oxide surfaces can be opposite in sign, and the positive oxide sites prevent the adsorption of cations but promote the adsorption of anions. Tagavifar et al.[8] have investigated the dependency of pH on the adsorption of anionic surfactants on Indiana limestone, and came to the conclusion that above pH 9 the adsorption decreased linearly with pH. They suggest that there are two adsorption mechanisms taking place: at lower pH values, charge regulation is the dominant mechanism, in which interaction between the surface and surfactant occurs by electrostatic attraction, and at higher pH values (nearing the pH_{pzc} of limestone), hydrogen bonding takes over as a regulating mechanism.[8] The ionic composition of the solution used for surfactant flooding was found to play a significant role in the loss of anionic surfactant to the reservoir.[4,7,16−18] Especially, the presence of monovalent and divalent cations has been a topic of extensive research in EOR. This is not entirely surprising, having

Received: October 12, 2018
Revised: January 9, 2019
Published: January 24, 2019

DOI: 10.1021/acs.energyfuels.8b03572
Energy Fuels 2019, 33, 805−813

seen that the ζ-potential can vary as a function of Ca^{2+}, one of the surface potential-determining ions (PDIs).[19]

Intuitively, when formulating a flooding solution a few notions ought to be considered. For one part, it is expected that monovalent cations, such as Na^+ and K^+, are less able to screen the surface charge than divalent cations, such as Ca^{2+} and Mg^{2+}, because of the latter's higher charge densities. This has the implication that divalent cations are able to act as ion bridges between a negatively charged surface and anionic surfactant. Second, a higher charge reduces the size of the double-layer or, in other words, leads to more effective screening of the surface charge. It may even cause reversal of the sign of the ζ-potential, further promoting the adsorption of the anionic surfactant to this originally negatively charged surface. Adsorption isotherm studies seem to confirm this and have shown that the addition of Na^+ increased the adsorption of sodium dodecyl sulfonate on graphitic material by 25%, whereas the addition of Ca^{2+} gave twice that amount.[18]

In general, it can be said that the adsorption of anionic surfactants is a mildly increasing function of ionic strength and divalent cation concentration.[8] The exchange of divalent cations from the flooding solution with other (monovalent) ionic species adsorbed to the mineral surface promotes the adsorption. Even though numerous studies corroborate these effects of ions in EOR as described above, it should be noted that the effects of the flooding composition remain highly specific to the crude oil properties and rock chemistry of the reservoir.[13]

To study the adsorption processes, it is important to have a model surface contacted to a transducing layer (allowing for rapid information interpretation). Model mineral materials can be obtained via, for example, atomic layer deposition,[20] grown at the surface from thin films formed by a layer-by-layer approach,[21] bulk synthesis,[22−24] or with the help of electrochemical methods. The latter are known as assisted approaches, as these are usually the products of electrochemical reactions that impose insulating deposit formation. Cathodic reduction (of e.g. protons, water, oxygen, nitrite) allows the local pH to increase, followed by, for example, silica deposition derived from the sol−gel processing.[25] In the presence of a templating agent, thin films with superior porosity characteristics can be formed.[26] Phenomenologically similar is the formation of calcite, which can be precipitated upon electrochemical pH modulation.[27−31] Electrochemistry can not only be used for model mineral deposition, but also to study the interfacial properties, such as charge transfer resistance, dielectric properties, or coverage estimation.

In order to study the adsorption process itself, there exist numerous techniques that allow for the estimation of the quantity of surfactant adsorbed to a given surface. One of the most intensively employed techniques is the quartz crystal microbalance (QCM), a tool that operates based on the converse piezoelectric effect. Adsorption of surfactant to the surface can be monitored via changes in the resonance (vibrational) frequency of the quartz crystal, and by this has allowed researchers to dynamically study the adsorption behavior.[32−34] Other tools that can be useful in this regard, in combination with QCM, are optical reflectometry[35,36] and atomic force microscopy.[37]

This work presents a simple method for the controlled deposition of calcite on a gold-finished QCM sensor, with the definitive purpose of being able to study adsorption behavior of an alcohol alkoxy sulphate (AAS) surfactant to the thus-deposited calcite. Model rock surface electrocrystallization followed by AAS surfactant adsorption studies were performed with the electrochemical QCM (EQCM). All aspects combined give a new methodology to study this complex adsorption process. First, electrocrystallization conditions were optimized and the established deposit was analyzed with electrochemical, spectroscopic, and imaging techniques. Following that, $CaCO_3$ particles were synthesized and their electrochemical surface properties (ζ-potential) were investigated when exposed to different experimental conditions (pH and pCa ($-\log[Ca^{2+}]$)). The effect of ionic strength and flooding solution composition on AAS adsorption to the calcite surface was finally measured with QCM.

2. EXPERIMENTAL SECTION

2.1. Chemicals. A 30 wt % alkaline AAS surfactant (mol. weight 700 g mol^{-1}; CMC = 0.035 wt %) solution was provided by Shell Global Solutions, which was diluted with Milli-Q water to a 15 wt % stock solution. Anhydrous ≥97.0% $CaCl_2$, ≥99.0% NaCl, ≥99.0% Na_2CO_3, powdered ≥99.5% $NaHCO_3$, anhydrous ≥98.0% NaOH pellets, ≥99.0% $K_4[Fe(CN)_6]$, pure CH_3COOH, and an 85 wt % solution H_3PO_4 were purchased from Sigma-Aldrich. Anhydrous ≥99.8% H_3BO_3 and ≥99.5% $NaNO_3$ were purchased from Merck. The pH of all working solutions was corrected with the aid of 28% NH_4OH or 1 M HCl solution.

2.2. Electrochemical Methods. All EQCM measurements (deposition and characterization) were performed using an EmStat3+ Blue from PalmSens. The Au-covered QCM sensor was mounted in the electrochemical cell module and served as the working electrode. A Pt plate and Ag/AgCl were also present in this module, being the counter and the reference electrodes, respectively. The electrochemically assisted calcite formation was performed at 25.1 °C in a supporting electrolyte containing either an excess of chloride (see column a—Table 1) or nitrate (see column b—Table 1). During electrochemical measurements, the flow passing the sensor surface was stopped.

Table 1. Composition of the "Deposition" Solutions Used To Study the Effect of the Anion (Chloride or Nitrate) on the Deposition Efficiency

	A (mM)	*B* (mM)	purpose
$CaCl_2$	50	50	Ca^{2+} supplier
NaCl	1000		background electrolyte
$NaNO_3$		1000	background electrolyte
$NaHCO_3$	25	25	CO_3^{2-} supplier

Linear sweep voltammetry (LSV) was conducted to find the optimal potential for the electrochemically assisted deposition. The EQCM was loaded with either solution A or B (see Table 1), and the potential was scanned from 0 to −1.5 V at a scan rate of 20 mV s^{-1}.

Chronoamperometry was conducted to perform the deposition. On the basis of the optimal potential as obtained from LSV, the oxygen (dissolved in the electrolyte solution) reduction potential was chosen and applied for 15−20 min. For this, the EQCM was loaded with a new batch of solution A or B (see Table 1).

To obtain information regarding the degree of deposited calcite surface coverage, cyclic voltammetry was performed on the sensor. The EQCM module was loaded with a 1 mM $K_4[Fe(CN)_6]$ and 500 mM Na_2SO_4 solution, and four cycles were run with a scan rate of 20 mV s^{-1} across the potential window of −0.3 to 0.6 V. The anodic and cathodic peak currents were compared to those prior to deposition, and their change was taken as an estimate for the degree of surface coverage.

2.3. Imaging and Spectroscopic Study. The morphology and elemental composition of the sensor deposits were studied with a JSM-6010LA InTouchScope using scanning electron microscopy (SEM)/energy-dispersive X-ray spectrometry (EDXS). The deposit on the sensor was characterized via SEM while operating under high voltage and vacuum mode at magnifications of 40−2500 times. Contrast

DOI: 10.1021/acs.energyfuels.8b03572
Energy Fuels 2019, 33, 805−813

micrographs were also taken to determine the (top view) surface coverage. This was done by mapping this micrograph to a binary color format, from which the occurrence of black and white spots was counted. The relative occurrence of black to white spots gave the percentage coverage. In addition, EDXS was employed to determine the ratio of elements Ca/C/O in the crystal deposits.

2.4. $CaCO_3$ Particle Synthesis and ζ-Potential Analysis. The effect of pH and pCa on the surface charge of $CaCO_3$ was studied. $CaCO_3$ microparticles (MPs) were prepared according to a modified protocol described by Babou-Kammoe et al.[38] In short, the MPs were obtained by a dropwise addition of a 0.1 M NaOH with 0.1 M $CaCl_2$ solution to a 0.1 M NaOH with 0.1 M Na_2CO_3 and 0.1 M NaCl solution. The only difference compared to the referred protocol is that here $CaCl_2$ was used as opposed to $Ca(NO_3)_2{\cdot}4H_2O$. The MPs were characterized with a Thermo Scientific Nicolet iS50FT-IR using KBr pellets in the weight ratio 1:4 (MPs/KBr).

For studying the pH dependency, a 0.01 M Britton-Robinson buffer was prepared by dissolving 0.684 mL 85 wt % H_3PO_4, 0.6183 g H_3BO_3, and 0.572 mL CH_3COOH in 250 mL of Milli-Q. Subsequently, 100 mg of $CaCO_3$ MPs was dispersed in this buffer. A 1 M NaOH solution was prepared with the sodium hydroxide pellets, and this was used to adjust the pH to the desired value (studied were pH 2, 4, 6, 7, 8, 9, 10, 11, and 12).

For studying the pCa dependency, a 500 mM stock solution of $CaCl_2$ with 0.1 mg/mL $CaCO_3$ MPs was prepared in Milli-Q. A blank stock solution of 0.1 mg/mL $CaCO_3$ MPs in Milli-Q was also prepared in order to create a dilution series in $[Ca^{2+}]$ of 500, 100, 50, 10, and 1 mM. These solutions were corrected to $9.45 \leq pH \leq 9.55$ with the aid of drops of concentrated ammonium hydroxide or hydrochloric acid during stirring (2000 rpm). The choice for 0.1 mg/mL stems from the advised concentration according to the manual of the Malvern Zetasizer Nano ZS.[39]

2.5. Quartz Crystal Microbalance. Adsorption measurements were made using a Q-Sense QCM from Biolin Scientific. The sensors for these measurements were AT-cut gold-coated quartz crystals 1 cm in diameter. The sensors were plasma-cleaned for 20 min, with a PDC-002-CE Plasma Cleaner by Harrick Plasma prior to installation in the QCM. All QCM measurements were run at a temperature of 23.4 °C. The liquid flow velocity passing the sensor was set at 200 μL min^{-1}.

To study the effects of sodium and calcium ions on the surfactant adsorption separately, the solution series as shown in Table 1 were prepared. These were made using NaCl and $CaCl_2$ and dissolving their appropriate amounts in Milli-Q water. All solutions were corrected to $9.45 \leq pH \leq 9.55$ with the aid of drops of concentrated ammonium hydroxide or hydrochloric acid during stirring (2000 rpm).

3. RESULTS AND DISCUSSION

3.1. Electrochemically Assisted Deposition. Electrocrystallization has gained a positive reputation for the formation of $CaCO_3$ deposits onto electrode materials, as it allows the control of the formation rate, amount, and even morphology of the crystals.[30,31] The trick is to create an alkaline environment at the liquid−solid interface of the sensor to favor the local precipitation of $CaCO_3$. Plasma-cleaned gold-coated QCM sensors were used as the working electrode in a three-electrode configuration setup. LSV was conducted at a scan rate of 20 mV s^{-1}, potential was swept from 0 to −1.5 V, with either 1 M NaCl or 1 M $NaNO_3$ as the background electrolyte (see also Table 2) to determine the optimal potential for the oxygen and nitrate reduction reactions.

$$O_2 + 2H_2O + 4e^- \rightarrow 4OH^- \quad (1)$$

$$NO_3^- + H_2O + 2e^- \rightarrow NO_2^- + 2OH^- \quad (2)$$

This is compensated at the anode by oxygen or chlorine evolution, with $NaNO_3$ or NaCl used as electrolyte, respectively. The resulting LSV profiles are shown in Figure 1a. As seen from the reaction products, hydroxide ions are generated at the cathode, and this induces the local deposition of $CaCO_3$ according to the two-step process

$$HCO_3^- + OH^- \rightarrow H_2O + CO_3^{2-} \quad (3)$$

$$Ca^{2+} + CO_3^{2-} \rightarrow CaCO_3 \quad (4)$$

At potentials lower than 1.23 V (vs NHE), water reduction, giving OH^- ions as the reaction products, is expected to occur

$$2H_2O + 2e^- \rightarrow H_2 + 2OH^- \quad (5)$$

To prevent this undesired hydrogen evolution, which can destabilize the formed $CaCO_3$ deposit,[40] it is good practice to set the cathodic potential not too negative.

Overall, the reduction currents are larger for the nitrate-based electrolyte (as both reduction reactions 1 and 2 can take place now), and this becomes especially prominent below −0.8 V. Both profiles exhibit the likely onset of hydrogen evolution at potentials below −1.2 V, substantiated by the fact that blackening of the electrode material was observed for large negative potentials (probably because of layer delamination by H_2 formation) and that no other species could explain the rapid increase in cathodic current.

The deposition process can be run in potentiostatic mode (e.g., chronoamperometry) to control the reduction reactions mentioned above. By coupling this process to QCM, the extent of deposition on the sensor surface can be monitored via the change in resonance frequency of the quartz crystal during the process. The selected potentials for electrodeposition were −1.2 V for both background electrolytes, in order to prevent the undesired hydrogen evolution (which may ruin the deposit by bubble formation). This potential was applied for 15 to 20 min during chronoamperometry, depending on when the frequency leveled off as observed with EQCM. The chronoamperograms are depicted in Figure 1b. The frequency change of the sensor was monitored in tandem, and is depicted in Figure 1c.

As expected, the current measured in the presence of nitrate is significantly larger in magnitude, which is in agreement with the voltammogram of Figure 1a. The chronoamperogram is equally congruent with the observed frequency change; the deposition evolves much further for the case with nitrate-based electrolyte. It is still remarkable to see that the $I-t$ curves in Figure 1b show an increasing magnitude of the cathodic current as the deposition progresses, which implies that the rate of deposition increased with time. By intuition, however, it is expected that the current becomes weaker as more surface area is covered by carbonate crystals. This is under the pretence of an insulating deposit. During the measurement, the crystals were most likely hydrated and still relatively porous. Moreover, in the presence of numerous nucleation sites at the electrode surface, $CaCO_3$ is

Table 2. Solution Composition for the Adsorption Studies To Measure the Effect of Sodium (Left Column) and Calcium Ion Concentrations (right Column)

flooding (mM) $[Na^+]$	solution I $[Ca^{2+}]$	flooding (mM) $[Na^+]$	solution II $[Ca^{2+}]$
500	50	100	500
100	50	100	100
50	50	100	50
10	50	100	10
1	50	100	1

DOI: 10.1021/acs.energyfuels.8b03572
Energy Fuels 2019, 33, 805−813

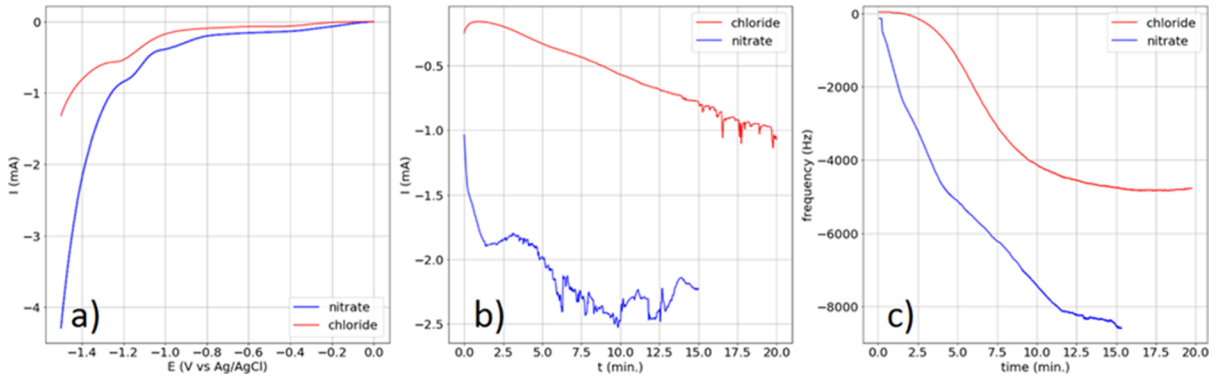

Figure 1. (a) LSV conducted in 1 M $NaNO_3$ (blue) or 1 M NaCl (red) background electrolyte with a scan rate equal to 20 mV s^{-1}; (b) chronoamperometric curves for the deposition process performed at −1.2 V, in N (blue, 15 min) or C (red, 20 min) electrolyte; (c) QCM-D frequency monitoring, synergistic to the chronoamperogram in (b).

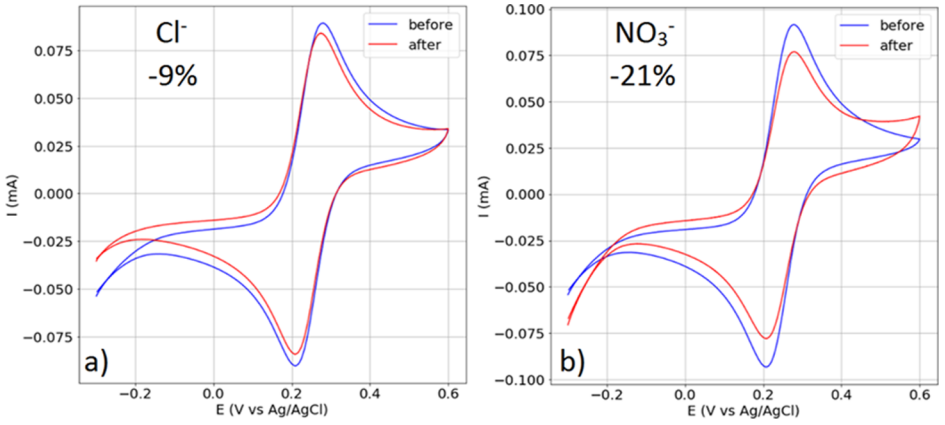

Figure 2. CVs for the reversible oxidation/reduction of ($[Fe(CN)_6^{3-/4-}]$ = 1 mM) at 20 mV s^{-1} on a gold QCM-D sensor before and after $CaCO_3$ deposition. Deposition in (a) chloride-based electrolyte and (b) nitrate-based electrolyte. The average percentage drop in peak currents is displayed in each box.

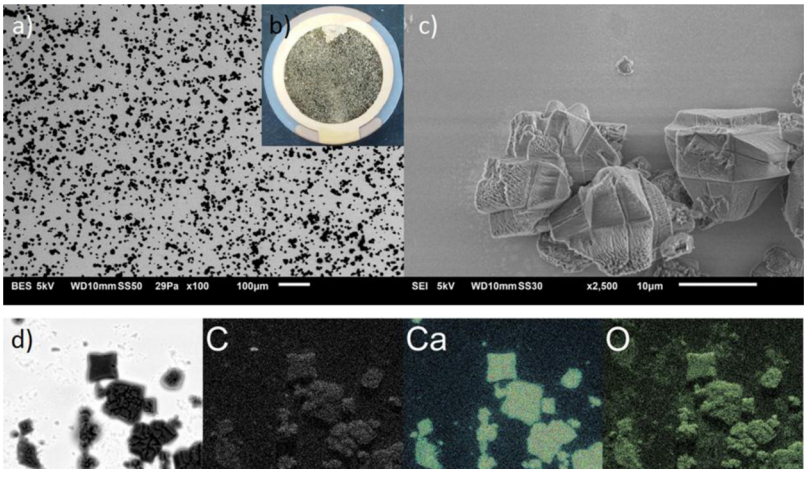

Figure 3. SEM and EDXS micrographs of $CaCO_3$ on a gold sensor made in the presence of sodium chloride as background electrolyte: (a) SEM contrast image (100× magnified, black spots indicate deposit); (b) photograph of the deposited QCM-D sensor; (c) SEM 2500× magnified; (d) EDXS of the elements of interest for $CaCO_3$ (brighter spots correspond to the indicated element).

additionally incorporated into the crystal lattice upon the Ca^{2+} reaction with the bicarbonate anions

$$Ca^{2+} + HCO_3^- \rightarrow CaCO_3 + H^+ \quad (6)$$

which leads to the additional formation of protons that can subsequently be reduced via

$$2H^+ + 2e^- \rightarrow H_2 \quad (7)$$

Hence, this could explain the gradual increase in current magnitude over time (see Figure 1b). The fluctuations in current at later times may be the consequence of emerging hydrogen gas bubbles. Probably, this has a disruptive effect on the performance of the oxygen and nitrate reduction reactions 1 and 2.

DOI: 10.1021/acs.energyfuels.8b03572
Energy Fuels 2019, 33, 805−813

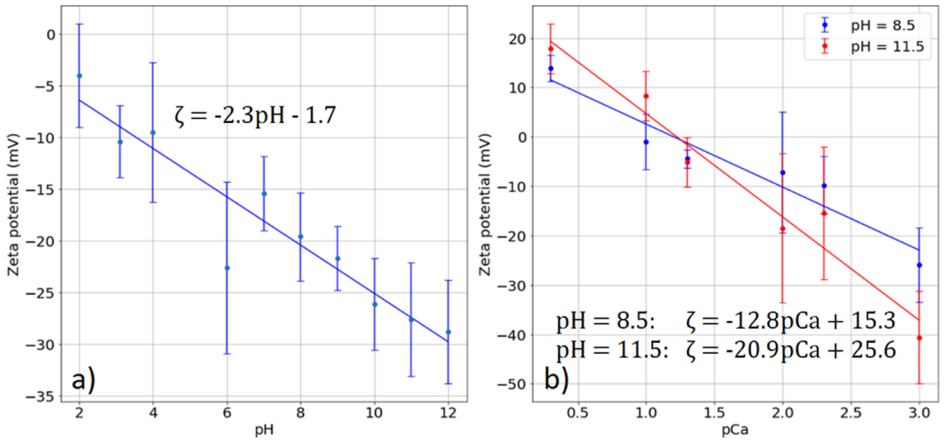

Figure 4. Variation in ζ-potential as a function of (a) pH in a Britton-Robinson buffer and (b) pCa for pH ~8.5 (blue) and pH ~11.5 (red) with $CaCl_2$ as background electrolyte. The equilibration time was 3 weeks.

3.2. $CaCO_3$ Deposit Characterization. Electrochemically formed model mineral rock deposits of $CaCO_3$ were characterized using electrochemistry, imaging, and spectroscopy techniques. First, the cyclic voltammogram (CV) has been recorded before and after the electrochemically assisted deposition of $CaCO_3$ on a gold-coated QCM sensor, in the presence of a reversible redox probe—ferrocyanide ($K_4[Fe(CN)_6]$). The drop in the faradaic peak current (measured as a difference between best fit of the capacitive current arm and the maximum peak point) can provide a measure of the degree of the reduction in electroactive surface area resulting from the insulating layer formation. The CVs before and after $CaCO_3$ formation are compared and shown in Figure 2. It is immediately noticeable that the ferrocyanide oxidation or ferricyanide reduction currents drop in the presence of electrocrystallized deposits. As expected, the reduction of faradaic current is larger for the deposit created in a nitrate-based electrolyte (−21% change—see Figure 2b) compared to −9% observed for $CaCO_3$ formed in the 1 M NaCl solution (see Figure 2a). This suggests a greater (insulating) coverage by $CaCO_3$ compared to the deposit created in the chloride-based electrolyte.

3.3. Morphological Study and Elemental Analysis. The SEM and EDXS micrographs in Figure 3 were taken to study the morphology and elemental composition of the deposit, respectively, and to get an estimate of the degree of surface coverage. Figure 3a shows an SEM contrast micrograph (see also Figure SI3 in the Supporting Information). This was mapped to a binary color format in ImageJ, after which the relative occurrence of black to white spots was counted. This produced a top-view coverage of 20%, which is in agreement with what Figure 2b shows, and slightly deviates from values obtained from the reduction of peak currents stated earlier in Figure 2a. This difference is most likely explained by the crystals having likely been hydrated during voltammetry, therefore being able to allow electrochemical species to diffuse to the electrode also via the crystals themselves. On the other hand, even though the top-view percentage gives information on the extent of coverage, it does not provide an accurate measure of the actual percentage of the surface shielded by the deposit.

As exemplified in Figure 3c, the majority of the crystal structures observed by SEM are of cubic and rhombic shape (see also Figure SI2 from the Supporting Information), with a dense packing. This suggests that the deposit is predominantly the mineral calcite rather than the thin needle-shaped aragonite. In addition, the EDS results in Figure 3d clearly verify the chemical nature of the crystalline species to be calcium carbonate. The composition, normalized to calcium, was determined to be Ca/C/O = 1:1.5:3.4.

Not all crystal faces show the same degree of smoothness. The coarser appearance on some faces is possibly a consequence of re-dissolution and recrystallization of the calcium carbonate, a hypothesis which is also suggested by Dinamani et al.[31] This behavior is likely due to the processing steps between deposition and SEM measurement (washing and drying).

3.4. Surface Charge Analysis. The dependence of calcite's surface charge on pH is still under active debate in the scientific community.[19,41] Various researchers have mapped the variation of the ζ-potential of natural and synthetic calcite as a function of electrolyte pH, but the results are ambiguous. The variability between the data sets can be attributed to the carbonate mineral being soluble in aqueous solutions across the pH range studied; thus, a dissolution equilibrium is established. This implies that the charge developed on the surface is also reliant on the sample history, equilibration time (the time between sample preparation and actual ζ-potential measurement), and choice of supporting electrolyte.[42]

Upon varying the pH while keeping the pCa constant, multiple researchers independently observed that the ζ-potential remained constant as well.[19] This led to the conclusion that it is rather the role of the surface lattice ions Ca^{2+} and CO_3^{2-} that determine the ζ-potential of calcite, according to surface complexation reactions[43] such as

$$-CO_3H + Ca^{2+} \leftrightharpoons -CO_3Ca^{+} + H^{+} \quad (8)$$

$$-CaOH + CO_3^{2-} \leftrightharpoons -CaCO_3^{-} + OH^{-} \quad (9)$$

Consequently, it can be stated that the fundamental PDIs are the earlier mentioned lattice ions, with H^+ and OH^- playing a secondary role.

$CaCO_3$ MPs were prepared according to the procedure in Section 2.4 and characterized by Fourier transform infrared (FT-IR) (see Supporting Information for the IR spectrum and SEM micrographs—Figure SI1). The major peaks for $CaCO_3$ appear at wavenumbers 715, 881, 1442, 1802, and 2526 cm^{-1}, which show accurate resemblance with the literature.[44,45] The observation of what was thought to be precipitation of $Ca(OH)_2$ during the synthesis could have contaminated the sample. However, the twin peaks at 881 and 715 cm^{-1} (fundamental

DOI: 10.1021/acs.energyfuels.8b03572
Energy Fuels 2019, 33, 805−813

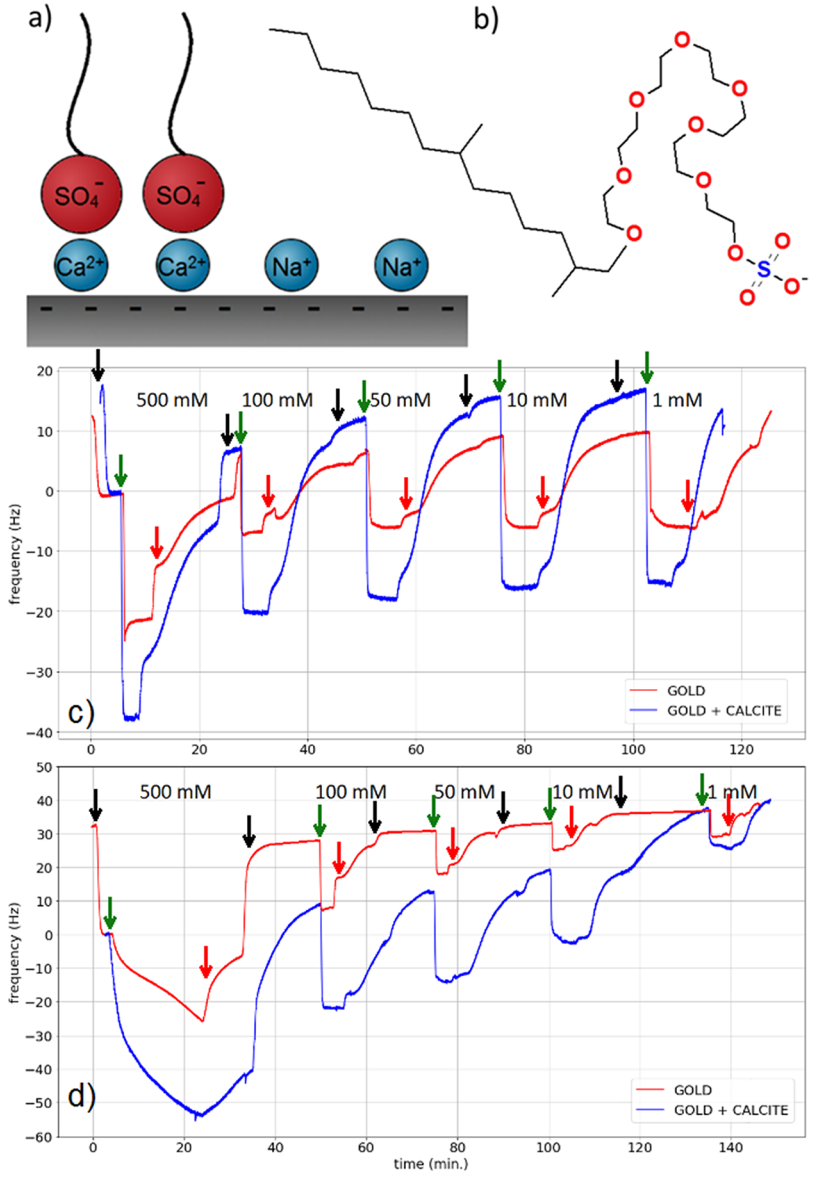

Figure 5. (a) Adsorption to the evenly charged surface bridged by divalent calcium ions; (b) schematic representation of the AAS surfactant; (c,d) QCM-D frequency monitoring for a calcite on a gold surface at pH 9.5 in the presence of 0.15 wt % surfactant, upon variation of (c) the Na^+ concentration and at constant Ca^{2+} concentration of 50 mM, and (d) Ca^{2+} concentration and at constant Na^+ concentration of 100 mM (millimolar concentrations indicated in the figure). Arrows indicate the times of addition of the corresponding brine solution (black), the addition of surfactant to this brine (green), and the removal of surfactant (red).

vibrations of the radical CO_3^{2-} species), and the lack of a prominent peak in the 3500−3000 cm^{-1} region (characteristic for O−H vibrations), provide ample evidence that this is the spectrum of nearly pure $CaCO_3$.

The ζ-potential of these particles was measured as a function of pH and pCa, and the results are shown in Figure 4. Linear regression lines have been fitted to the data, which lie for all but one data point within the error bars.

As was postulated in the Introduction, it is expected that Ca^{2+} is an important PDI for the carbonate surface. This is indeed reflected in the results shown in Figure 4b, as both data sets show a significant ζ-potential dependency on pCa. At low pCa, the ζ-potential is positive, corresponding to the occurrence of surface complexation reactions akin to 8 and 9.

Regardless of the pH, both data sets show within experimental error a similar ζ-potential change versus pCa. At pH 11.5, the magnitudes of the ζ-potential do however seem to be larger. This is as expected for high pCa, and the increased $[OH^-]$ makes the ζ-potential more negative. The more positive ζ-potential in the low pCa region at pH 11.5 may be attributable to an increased occurrence of $-CO_3Ca^+$ sites on the surface (eq 8).

The approximate independency of ζ-potential to pH has been observed before in the literature.[19] The actual values for the potential are difficult to compare with those of other studies, because these are highly dependent on sample history, choice of electrolyte, and equilibration time (being 3 weeks in the case of this work).

Interestingly, the isoelectric point (IEP) read out from the ζ-potential plotted against the pCa seems to coincide for both pH conditions, which suggests that in the presence of Ca^{2+} the IEP is weakly dependent on pH and is dominated by the pCa. From the data presented in Figure 4b, the IEP is located at pCa ≈ 1.2

DOI: 10.1021/acs.energyfuels.8b03572
Energy Fuels 2019, 33, 805−813

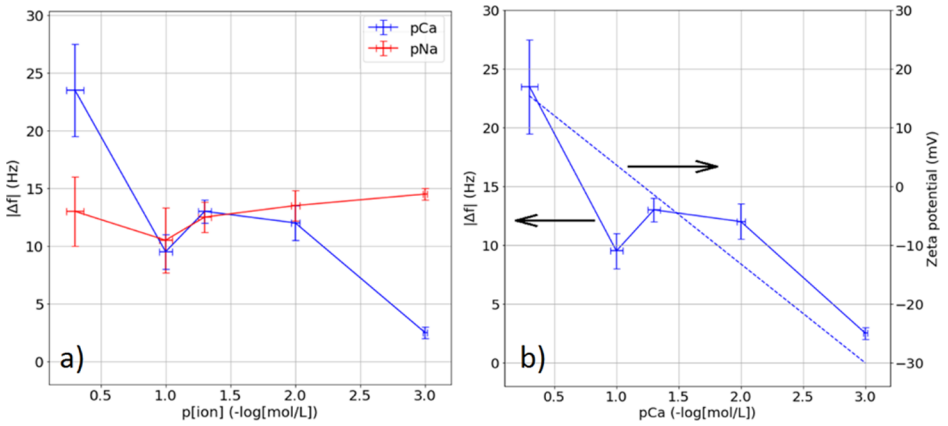

Figure 6. Variation in absolute frequency, corrected for a bare gold background, versus (a) pNa and pCa on calcite, for the two different cases seen in Figure 5; (b) frequency change and the ζ-potential of calcite (dotted line) as a function of pCa.

($[Ca^{2+}] \approx 60$ mM). This is at a lower concentration compared to that reported by Al Mahrouqi et al.[19] At the same time, values of pCa ≈ 0.75 ($[Ca^{2+}] \approx 180$ mM) and pCa > 2 have been reported by others.[42,46] The most straightforward reason for this broad range of reported IEP values may be the different background electrolytes employed in the experiments, but this is not the only factor. For instance, Chen et al.[46] performed comparable experiments with deionized water, in which they dissolved $CaCl_2$ to vary the pCa. Their IEP values are in the range pCa = 0.20−0.75, but it could not be extracted from their paper what their equilibration time of the sample was.

This comparison with other studies persuades to assume that the data collected here are distinct for the operating conditions of this experiment, and that care should be taken if one attempts to map these data to different conditions. Adsorption studies with calcite (next section) have therefore been conducted with the same conditions of pCa and pH.

3.5. Surfactant Adsorption Study. In Figure 5c,d, the results of the dynamic adsorption experiment by QCM of the anionic AAS surfactant on calcite versus bare gold are presented. In theory, the amount of surfactant adsorbed to the surface can be calculated from the change in resonance frequency, as described by the Sauerbrey equation.[47] However, many more factors play a role in establishing this resonance frequency, such as compression effects by pressure differences, and viscosity and density changes in the fluid contacting the crystal surface.[7] This makes the mass to frequency relationship nonlinear under experimental conditions, as opposed to the theoretical Sauerbrey equation. With a lack of information on all these effects, the results in this work refrain from making quantitative statements regarding the adsorbed mass.

The data sets shown in Figure 5c,d entail the 5th overtone of the fundamental resonance frequency of the crystal sensor. For each set of flooding parameters, the sensor was first flushed with only the brine (consisting of NaCl and $CaCl_2$), after which it was flushed with brine containing 0.15 wt % AAS ($[AAS] \approx 2.1$ mM; for its molecular structure, see Figure 5b). Removal of the adsorbed surfactant was effected again by flushing with only brine.

By comparison, from the difference in frequency drop between the two frequency versus time (f−t) curves in Figure 5c,d, it becomes obvious that the presence of calcite on the sensor surface has a profound effect on the extent of AAS adsorption. The desorption process appears to be characterized by an initial jump in frequency, followed by a gradual decrease to the original value. At this point, we can only speculate what might happen here. There is a fast process and there is a slow process. The fast process is suggested to come from the release of weakly bound micelles, and the slow process is suggested to come from the release of surfactant molecules more strongly and directly bound to the calcite surface as bilayer lamella.

To better project and contrast the actual effect of calcite on AAS surfactant adsorption, Figure 6a has been constructed. Here, the absolute change in resonance frequency, as extracted from Figure 5c,d, has been mapped versus pNa ($-\log[Na^+]$) or pCa.

It becomes noticeable that the adsorption remains relatively constant when the pNa is varied, with $[Ca^{2+}]$ fixed at 50 mM. If the ζ-potential is indifferent to the pNa, as has been found before,[19] then the calcite surface is close to the IEP (see also Figure 4b). Then, electrostatics would play a minor role and it is indeed expected that there is hardly any variation in adsorption across the concentration range studied.

Upon variation of the pCa (with $[Na^+]$ fixed at 100 mM), it is seen that increasing the $[Ca^{2+}]$ in the brine solution does show an increase in AAS adsorption. This observation is likely to be due to the ion-bridging properties of Ca^{2+} (see Figure 5a). It is expected that electrostatics do play a significant role in the adsorption behavior in this case, as it was observed that the ζ-potential of calcite is a strong function of pCa. In Figure 6b, the frequency decrease (increase of adsorbed mass of AAS) and change of ζ-potential (becomes more positive) as functions of pCa are shown.

It is evident that at a high pCa, AAS adsorption is almost negligible on calcite. This is mainly due to a negatively charged surface with hardly any bound Ca^{2+}, required for adsorption of the surfactant. Starting from pCa > 10 mM, the surface is able to bind AAS. In the intermediate regime (1.0 < pCa < 2.0), pCa has hardly any effect on the AAS absorption and ζ-potential, which is close to the IEP. In this regime, electrostatic interactions are apparently of minor importance.

4. CONCLUSIONS

In this work, we have successfully deposited calcite crystals on a gold-coated QCM sensor using an electrochemically assisted method. These calcite-modified sensors were investigated as a model substrate for calcite rock in the adsorption of AAS surfactants. This unique combination opens a new methodology to study adsorption phenomena. In the surfactant flooding process of EOR, surfactant loss is a serious problem and better

DOI: 10.1021/acs.energyfuels.8b03572
Energy Fuels 2019, 33, 805−813

understanding of this phenomenon might be of use when proposing mitigations. The effect of supporting electrolyte, deposition potential, and time were optimized, yielding a calcite deposit compatible with the QCM measurement. SEM and EDX were used to investigate the morphology of the deposited calcite (cubic and rhombic crystal shapes were observed) and elemental composition, respectively.

It was determined through the measurement of the ζ-potential that the IEP of the calcite is dependent of pCa, with an IEP at approximately pCa $\approx$ 1.2 ($[Ca^{2+}] \approx 60$ mM) in alkaline conditions. It was also observed that the ζ-potential becomes increasingly more negative with increasing pH. This shows that Ca^{2+} is a primary PDI and determines the sign (and magnitude) of the ζ-potential under the alkaline conditions of interest.

The sensitivity of the ζ-potential to variations of pCa is reflected in the adsorption behavior of the AAS surfactant. For varying pNa, the adsorption remained relatively constant, but when varying the pCa, adsorption increases for higher concentrations. An interesting observation made is that the adsorption remained quite constant for pCa = 1−2 (based on our ζ-potential measurements, the calcite surface is close to the IEP ($\pm$10 mV) for these concentrations). This suggests that in the absence of a prominent electrostatic gradient, adsorption of the AAS surfactant is indifferent to calcite. Despite this indifference, adsorption was still significant (10−15 Hz frequency shift), meaning that electrostatic effects remain important in both the maximization and minimization of adsorption to calcite.

The work presented here can potentially be extended to the deposition of different other minerals and metal oxides on QCM sensors. Moreover, the electrochemically assisted deposition has also a potential for depositing heterogeneous minerals, which we are currently studying.

■ ASSOCIATED CONTENT

Supporting Information

The Supporting Information is available free of charge on the ACS Publications website at DOI: 10.1021/acs.energyfuels.8b03572.

IR spectrum of $CaCO_3$ MPs; SEM image of $CaCO_3$ MPs; additional SEM images of the $CaCO_3$ deposit on QCM sensors (PDF)

■ AUTHOR INFORMATION

Corresponding Authors

*E-mail: N.Kumar-2@tudelft.nl (N.K.).
*E-mail: L.Poltorak@tudelft.nl (L.P.).

ORCID

Lukasz Poltorak: 0000-0002-8799-8461
Ernst J. R. Sudhölter: 0000-0003-3296-953X

Notes

The authors declare no competing financial interest.

■ ACKNOWLEDGMENTS

The authors thank Dr. M. Brewer and Dr. J. van Wunnik (Shell Global Solutions) for providing surfactant samples and for their active discussions. Financial support was provided by Shell Global Solutions.

■ REFERENCES

(1) Shell. EONORDET Surfactants for EOR, 2013.
(2) Negin, C.; Ali, S.; Xie, Q. Most Common Surfactants Employed in Chemical Enhanced Oil Recovery. *Petroleum* **2017**, *3*, 197−211.
(3) Amirianshoja, T.; Junin, R.; Kamal Idris, A.; Rahmani, O. A Comparative Study of Surfactant Adsorption by Clay Minerals. *J. Pet. Sci. Eng.* **2013**, *101*, 21−27.
(4) Liu, Q.; Dong, M.; Zhou, W.; Ayub, M.; Zhang, Y. P.; Huang, S. Improved Oil Recovery by Adsorption-Desorption in Chemical Flooding. *J. Pet. Sci. Eng.* **2004**, *43*, 75−86.
(5) Schlumberger. Carbonate Reservoirs: Meeting Unique Challenges to Maximize Recovery. *Schlumberger Mark. Analysis*, 2007; pp 1−12.
(6) Sloan, R. Quantification of Uncertainty in Recovery Efficiency Predictions: Lessons Learned from 250 Mature Carbonate Fields. *SPE Annual Technical Conference and Exhibition*, 2003.
(7) Ray, S. J.; Counce, R. M.; Morton, S. A. Effects of Electrolyte Concentration on Surfactant Adsorption to a QCM Immersed in Surfactant + Electrolyte Solutions. *Sep. Sci. Technol.* **2008**, *43*, 2489−2502.
(8) Tagavifar, M.; Jang, S. H.; Sharma, H.; Wang, D.; Chang, L. Y.; Mohanty, K.; Pope, G. A. Effect of PH on Adsorption of Anionic Surfactants on Limestone: Experimental Study and Surface Complexation Modeling. *Colloids Surf., A* **2018**, *538*, 549−558.
(9) Liu, X.; Yan, W.; Stenby, E. H.; Thormann, E. Release of Crude Oil from Silica and Calcium Carbonate Surfaces: On the Alternation of Surface and Molecular Forces by High- and Low-Salinity Aqueous Salt Solutions. *Energy Fuels* **2016**, *30*, 3986−3993.
(10) Budhathoki, M.; Barnee, S. H. R.; Shiau, B.-J.; Harwell, J. H. Improved Oil Recovery by Reducing Surfactant Adsorption with Polyelectrolyte in High Saline Brine. *Colloids Surf., A* **2016**, *498*, 66−73.
(11) Ma, K.; Cui, L.; Dong, Y.; Wang, T.; Da, C.; Hirasaki, G. J.; Biswal, S. L. Adsorption of Cationic and Anionic Surfactants on Natural and Synthetic Carbonate Materials. *J. Colloid Interface Sci.* **2013**, *408*, 164−172.
(12) Jian, G.; Puerto, M. C.; Wehowsky, A.; Dong, P.; Johnston, K. P.; Hirasaki, G. J.; Biswal, S. L. Static Adsorption of an Ethoxylated Nonionic Surfactant on Carbonate Minerals. *Langmuir* **2016**, *32*, 10244−10252.
(13) Yildiz, H. O.; Morrow, N. R. Effect of Brine Composition on Recovery of Moutray Crude Oil by Waterflooding. *J. Pet. Sci. Eng.* **1996**, *14*, 159−168.
(14) He, K.; Yue, Z.; Fan, C.; Xu, L. Minimizing Surfactant Adsorption Using Polyelectrolyte Based Sacrificial Agent: A Way to Optimize Surfactant Performance in Unconventional Formations. *SPE International Symposium on Oilfield Chemistry*, 2015.
(15) Kosmulski, M. The pH-dependent surface charging and points of zero charge. *J. Colloid Interface Sci.* **2011**, *353*, 1−15.
(16) Austad, T.; Rezaeidoust, A.; Puntervold, T. Chemical Mechanism of Low Salinity Water Flooding in Sandstone Reservoirs. *Society of Petroleum Engineers*, 2010; Vol. *129767* (September), pp 19−22.
(17) Moustafa, E. A. A. A.; Shedid, S. A. Effects of Magnesium and Potassium Sulfates on Oil Recovery by Water Flooding. *Egypt. J. Pet.* **2018**, *27*, 649.
(18) Wanless, E. J.; Ducker, W. A. Weak Influence of Divalent Ions on Anionic Surfactant Surface-Aggregation. *Langmuir* **1997**, *13*, 1463−1474.
(19) Al Mahrouqi, D.; Vinogradov, J.; Jackson, M. D. Zeta Potential of Artificial and Natural Calcite in Aqueous Solution. *Adv. Colloid Interface Sci.* **2017**, *240*, 60−76.
(20) Nilsen, O.; Fjellvåg, H.; Kjekshus, A. Growth of Calcium Carbonate by the Atomic Layer Chemical Vapour Deposition Technique. *Thin Solid Films* **2004**, *450*, 240−247.
(21) Ramos, A. P.; Doro, F. G.; Tfouni, E.; Gonçalves, R. R.; Zaniquelli, M. E. D. Surface Modification of Metals by Calcium Carbonate Thin Films on a Layer-by-Layer Polyelectrolyte Matrix. *Thin Solid Films* **2008**, *516*, 3256−3262.
(22) Stöber, W.; Fink, A.; Bohn, E. Controlled growth of monodisperse silica spheres in the micron size range. *J. Colloid Interface Sci.* **1968**, *26*, 62−69.

DOI: 10.1021/acs.energyfuels.8b03572
Energy Fuels 2019, 33, 805−813

(23) Boyjoo, Y.; Pareek, V. K.; Liu, J. Synthesis of Micro and Nano-Sized Calcium Carbonate Particles and Their Applications. *J. Mater. Chem. A* **2014**, *2*, 14270−14288.
(24) Abdel-Aal, N.; Satoh, K.; Sawada, K. Study of the adhesion mechanism of CaCO3 using a combined bulk chemistry/QCM technique. *J. Cryst. Growth* **2002**, *245*, 87−100.
(25) Shacham, R.; Avnir, D.; Mandler, D. Electrodeposition of Methylated Sol-Gel Films on Conducting Surfaces. *Adv. Mater.* **1999**, *11*, 384−388.
(26) Walcarius, A.; Sibottier, E.; Etienne, M.; Ghanbaja, J. Electrochemically Assisted Self-Assembly of Mesoporous Silica Thin Films. *Nat. Mater.* **2007**, *6*, 602−608.
(27) Devos, O.; Gabrielli, C.; Tlili, M.; Tribollet, B. Nucleation-Growth Process of Scale Electrodeposition. *J. Electrochem. Soc.* **2003**, *150*, C494−C501.
(28) Xu, S.; Melendres, C. A.; Park, J. H.; Kamrath, M. A. Structure and Morphology of Electrodeposited CaCO[sub 3]: X-Ray Diffraction and Microscopy Studies. *J. Electrochem. Soc.* **1999**, *146*, 3315−3323.
(29) Simpson, L. J. Electrochemically generated CaCO3 deposits on iron studied with FTIR and Raman spectroscopy. *Electrochim. Acta* **1998**, *43*, 2543.
(30) Rakitin, A. R.; Kichigin, V. I. Electrochemical Study of Calcium Carbonate Deposition on Iron. Effect of the Anion. *Electrochim. Acta* **2009**, *54*, 2647−2654.
(31) Dinamani, M.; Kamath, P. V.; Seshadri, R. Electrochemical Synthesis of Calcium Carbonate Coatings on Stainless Steel Substrates. *Mater. Res. Bull.* **2002**, *37*, 661−669.
(32) Keleşoğlu, S.; Volden, S.; Kes, M.; Sjöblom, J. Adsorption of Naphthenic Acids onto Mineral Surfaces Studied by Quartz Crystal Microbalance with Dissipation Monitoring (QCM-D). *Energy Fuels* **2012**, *26*, 5060−5068.
(33) Gabrielli, C. Quartz Crystal Microbalance Investigation of Electrochemical Calcium Carbonate Scaling. *J. Electrochem. Soc.* **1998**, *145*, 2386.
(34) Abudu, A.; Goual, L. Adsorption of Crude Oil on Surfaces Using Quartz Crystal Microbalance with Dissipation (QCM-D) under Flow Conditions†. *Energy Fuels* **2009**, *23*, 1237−1248.
(35) Dijt, J. C.; Stuart, M. A. C.; Fleer, G. J. Reflectometry as a Tool for Adsorption Studies. *Adv. Colloid Interface Sci.* **1994**, *50*, 79−101.
(36) Maroni, P.; Montes Ruiz-Cabello, F. J.; Cardoso, C.; Tiraferri, A. Adsorbed Mass of Polymers on Self-Assembled Monolayers: Effect of Surface Chemistry and Polymer Charge. *Langmuir* **2015**, *31*, 6045−6054.
(37) Al-Hashmi, A. R.; Luckham, P. F.; Heng, J. Y. Y.; Al-Maamari, R. S.; Zaitoun, A.; Al-Sharji, H. H.; Al-Wehaibi, T. K. Adsorption of High-Molecular-Weight EOR Polymers on Glass Surfaces Using AFM and QCM-D. *Energy Fuels* **2013**, *27*, 2437−2444.
(38) Babou-Kammoe, R.; Hamoudi, S.; Larachi, F.; Belkacemi, K. Synthesis of CaCO3 nanoparticles by controlled precipitation of saturated carbonate and calcium nitrate aqueous solutions. *Can. J. Chem. Eng.* **2011**, *90*, 26−33.
(39) Malvern instruments. Zetasizer Nano Series User Manual. Department of Biochemistry Biophysics Facility, University of Cambridge, 2004; No. 2, p 207.
(40) Plowman, B. J.; Jones, L. A.; Bhargava, S. K. Building with Bubbles: The Formation of High Surface Area Honeycomb-like Films via Hydrogen Bubble Templated Electrodeposition. *Chem. Commun.* **2015**, *51*, 4331−4346.
(41) Alroudhan, A.; Vinogradov, J.; Jackson, M. D. Zeta Potential of Intact Natural Limestone: Impact of Potential-Determining Ions Ca, Mg and SO4. *Colloids Surf., A* **2016**, *493*, 83−98.
(42) Thompson, D. W.; Pownall, P. G. Surface Electrical Properties of Calcite. *J. Colloid Interface Sci.* **1989**, *131*, 74−82.
(43) Song, J.; Zeng, Y.; Wang, L.; Duan, X.; Puerto, M.; Chapman, W. G.; Biswal, S. L.; Hirasaki, G. J. Surface complexation modeling of calcite zeta potential measurements in brines with mixed potential determining ions (Ca2+, CO32−, Mg2+, SO42−) for characterizing carbonate wettability. *J. Colloid Interface Sci.* **2017**, *506*, 169−179.
(44) Adler, H. H.; Kerr, P. F. Infrared Study of Aragonite and Calcite. *Am. Mineral.* **1962**, *47*, 700−717.
(45) Miller, F. A.; Wilkins, C. H. Infrared Spectra and Characteristic Frequencies of Inorganic Ions. *Anal. Chem.* **1952**, *24*, 1253−1294.
(46) Chen, L.; Zhang, G.; Wang, L.; Wu, W.; Ge, J. Zeta Potential of Limestone in a Large Range of Salinity. *Colloids Surf., A* **2014**, *450*, 1−8.
(47) Sauerbrey, G. Verwendung von Schwingquarzen Zur Wägung Dünner Schichten Und Zur Mikrowägung. *Z. Phys.* **1959**, *155*, 206−222.

DOI: 10.1021/acs.energyfuels.8b03572
Energy Fuels 2019, 33, 805−813